


Localization-delocalization transition in discrete-time quantum walks with long-range correlated disorder

C. V. C. Mendes, G. M. A. Almeida, M. L. Lyra, and F. A. B. F. de Moura*

Instituto de Física, Universidade Federal de Alagoas, 57072-900 Maceió, AL, Brazil

 (Received 18 October 2018; revised manuscript received 11 January 2019; published 12 February 2019)

We study the effects of spatially long-range correlated phase disorder on the Hadamard quantum walk on a line. The shift operator is built to exhibit an intrinsic disorder distribution featuring long-range correlations. To impose such, we resort to fractional Brownian motion with power-law spectrum $1/k^{2\alpha}$ with $\alpha \geq 0$ being the exponent that controls the degree of correlations. We discuss the scaling behavior of the walker's wave packet and report a localization-delocalization transition controlled by α . We unveil two intermediate dynamical regimes between exponential localization and full delocalization.

DOI: [10.1103/PhysRevE.99.022117](https://doi.org/10.1103/PhysRevE.99.022117)

I. INTRODUCTION

Quantum walk is the quantum mechanical analog of the classical random walk. Interest in the subject emerged roughly three decades ago after Aharonov *et al.* [1] put forward the main idea. As classical random walks have been of great utility in computer science, quantum walks are a formidable tool for designing quantum algorithms and for running quantum simulations (see Refs. [2,3] for reviews of the subject).

One of its main features is that the particle's wave function spreads out ballistically (rather than diffusively) on a regular lattice due to intrinsic quantum interference effects. Thereby, quantum walks yield significantly faster hitting times when compared to the classical case and thus readily find applications in quantum search problems [4–6]. Moreover, it was shown that quantum walks feature the necessary ingredients for universal quantum computation [7,8].

Quantum walks can be divided into two main kinds. Continuous-time quantum walks [9] are performed by defining a hopping Hamiltonian on a chosen graph and letting the system evolve through the Schrödinger equation. In a discrete-time quantum walk (DTQW) [1], the standard underlying mechanism consists of a set of internal degrees of freedom (e.g., spin) being the coin space (not necessarily being restricted to a two-dimensional subspace) alongside a configuration space denoting the walker's position. The protocol itself is triggered by repeatedly executing a “coin toss”—a unitary transformation acting on the coin space that scrambles wave-function components—followed by a conditional displacement obeying the coin state. Experimentally, this can be implemented using, e.g., NMR [10], ion traps [11], waveguide arrays [12,13], and superconducting devices [14].

The freedom in setting up the coin entails that very rich dynamics can be generated from rather simple rules thereby allowing one to obtain a handful of dynamical regimes at will [15]. After all, DTQWs can also be seen as a quantum cellular automaton [16]. Moreover, the interest in this kind of

procedure is far from being restricted to single-particle dynamics. Quantum walks of two interacting or noninteracting particles have also been addressed [17–21] and proved to be experimentally feasible [13,22]. This opens up the possibility of probing multiparticle entanglement and the role of interactions between them and, due to its greater complexity, may also be useful to deal with challenging computational tasks such as the graph isomorphism problem [23,24].

DTQWs then provide a powerful framework for studying complex quantum behavior, including decoherence [25], strongly correlated phenomena [26,27], topological phases [14,28–32], and localization [28,31,33–39], to name a few. This last in particular has been a relevant subject with some experiments being carried out [40,41]. In general, we expect the walker to undergo Anderson localization when subjected to disorder. It thus becomes important to find out how the transport properties of DTQWs are affected against different forms of noise.

In Refs. [28,31] the authors addressed dynamical regimes where Anderson localization in a DTQW is bypassed even in the presence of disorder, with the wave function avoiding complete trapping over a finite region of lattice. They further explained it in terms of topological phases of the quantum walk. Another remarkable feature in particular, as showed by Vieira *et al.* [42], is displayed by a class of dynamically disordered one-dimensional (1D) DTQWs in which spin-position entanglement reaches its maximum asymptotically for any input, thus outperforming its ordered counterpart. This was further investigated including fluctuating and static disorder [43], and an experiment has recently been performed in a photonic platform [44].

These examples make the case that disorder can be a handy resource, especially when one has some degree of control over it. Properly tailored disordered DTQWs thus possess enormous potential in quantum information processing. Our goal here is to unveil transport properties of a class of correlated, static disorder known for inducing a localization-delocalization transition [45].

In condensed matter physics, the breakdown of Anderson localization can be spotted in 1D tight-binding models with

*fidelis@fis.ufal.br

disorder featuring short- [46,47] or long-range correlations [45,48]. The latter was found to undergo a metal-insulator transition with sharp mobility edges indicating the presence of extended states [45,48]. Its rich dynamics has been exploited since then in various frameworks [49–55], including experimental verification using waveguides [56,57]. The interplay between localization and delocalization also finds use in quantum-communication tasks such as entanglement distribution [54] and quantum-state transfer [55].

In this work we aim to explore the wave-packet dynamics of a 1D DTQW embedded with long-range correlations following a power law encoded as on-site static phase disorder [39] in the conditional translation operator. In our calculations, the shift operator is built using as the source of disorder a fractional Brownian motion with power-law spectrum having a characteristic exponent α accounting for the degree of correlations within the shift unitary operator ($\alpha \geq 0$). In particular, we rely on finite-size scaling analysis to characterize the transition from exponential localization to delocalization of the walker's wave packet.

II. MODEL AND FORMALISM

We deal with a Hadamard quantum walk on an open line. Let H_p be the Hilbert space spanned by the positions $\{|n\rangle\}$ ($n = 1, 2, \dots, N$) of the particle alongside a two-level coin space defined by H_C . This last may be associated with internal degrees of freedom of the walker, say, its spin ($|\uparrow\rangle, |\downarrow\rangle$). The total Hilbert space of the quantum walk is thus $H = H_C \otimes H_p$. The evolution for a given initial state $|\psi(t=0)\rangle$ can be evaluated using a unitary operator U defined as $U = S(C \otimes I)$ where S is the conditional translation operator including on-site static phase disorder [39],

$$S = |\uparrow\rangle\langle\uparrow| \sum_n (e^{i2\pi\zeta_{n+1}} |n+1\rangle\langle n|) + |\downarrow\rangle\langle\downarrow| \sum_n (e^{i2\pi\zeta_{n-1}} |n-1\rangle\langle n|), \quad (1)$$

with ζ_n denoting the disordered phase, and C being the Hadamard coin operator,

$$C = \frac{1}{\sqrt{2}} \begin{pmatrix} 1 & 1 \\ 1 & -1 \end{pmatrix}. \quad (2)$$

The quantum state of the walker at the time t is given by $|\psi(t)\rangle = U^t |\psi(t=0)\rangle$. In this work, ζ_n takes values obtained from a disorder distribution with intrinsic long-range correlations. To generate these numbers we consider the trace of the fractional Brownian motion defined by [45]

$$V_n = \sum_{k=1}^{N/2} \frac{1}{k^\alpha} \cos\left(\frac{2\pi nk}{N} + \phi_k\right), \quad (3)$$

where ϕ_k represents a random phase distributed within the range $[0, 2\pi]$. We emphasize that the sequence $\{V_n\}$ features a power spectrum of approximately $1/k^{2\alpha}$ [45]. For $\alpha = 0$, the sequence is fairly uncorrelated. On the other hand, $\alpha > 0$ introduces long-range correlations in $\{V_n\}$. Therefore, exponent α ultimately controls the degree of correlations within the disordered sequence. In addition, hereafter we normalize

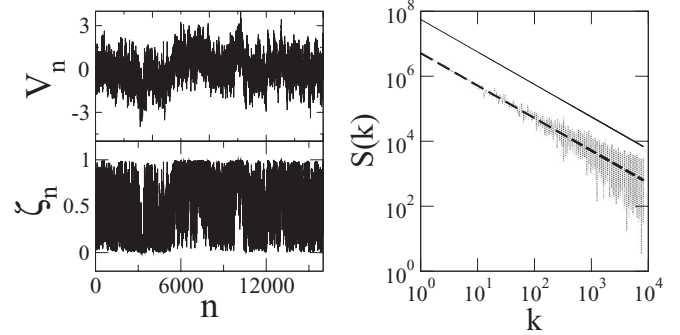


FIG. 1. Left: V_n and ζ_n landscapes for a chain with $N = 16000$ sites and $\alpha = 0.5$. The mapping transformation restricts ζ_n to the interval $[0, 1]$. Right: Spectral densities of the potential landscapes. V_n has a pure power-law spectrum (solid line). The spectral density of ζ_n exhibits the same overall power-law decay with random fluctuations. The dashed line is a guide for the eye.

$\{V_n\}$ so that $\langle V_n \rangle = 0$ and $\langle V_n^2 \rangle = 1$. This effectively modifies the disorder strength locally while keeping the global disorder strength the same for any α [58].

With all that set up, we define $\zeta_n = 0.5 \tanh(V_n) + 0.5$ to adjust the range of the correlated disordered phases within the interval $[0, 2\pi]$. We stress that this transformation does not change the asymptotic correlation function of the sequence. In Fig. 1 we illustrate this aspect by plotting both V_n and ζ_n together with their respective spectral densities for the particular case of $\alpha = 0.5$. Note that both series have a power-law spectrum, and the mapping between them only adds random fluctuations to the overall $1/k$ decay. The resulting series develops distinct statistical properties depending on the value of α . For $\alpha < 1/2$ it remains statistically stationary. For $1/2 < \alpha < 3/2$ it generates a landscape with a fractional dimensionality and Hurst exponent $H = \alpha - 1/2$ [59]. This implies that the series is similar to the trace of a fractional Brownian motion with antipersistent increments for $1/2 < \alpha < 1$ and persistent increments for $1 < \alpha < 3/2$. For larger values of α the series has $H = 1$ and the underlying disorder becomes irrelevant. In what follows we show that the dynamics of the quantum walker is strongly dependent on the statistical regime of the random phase landscape.

Most of our analysis is made upon the wave-packet spreading

$$\sigma(t) = \sqrt{\sum_n [n - \langle n(t) \rangle]^2 P_n(t)}, \quad (4)$$

where $P_n(t) = |\langle \psi(t) | \uparrow, n \rangle|^2 + |\langle \psi(t) | \downarrow, n \rangle|^2$ is the probability of the walker to be found at the n th site and $\langle n(t) \rangle = \sum_n n P_n(t)$ is the walker's mean position. In short, σ measures the width of the wave packet. This piece of information allows us to tell about how fast it goes over time as well as its localization properties. The latter can be inferred from a finite-size scaling analysis. If, after a very long time, $\sigma \propto N$ (σ remains constant), this means delocalization (localization). Further, $\sigma \propto t^1$ indicates ballistic dynamics with constant velocity while $\sigma \propto t^{1/2}$ points to diffusive spreading. Now equipped with the tools above, we are ready to perform a

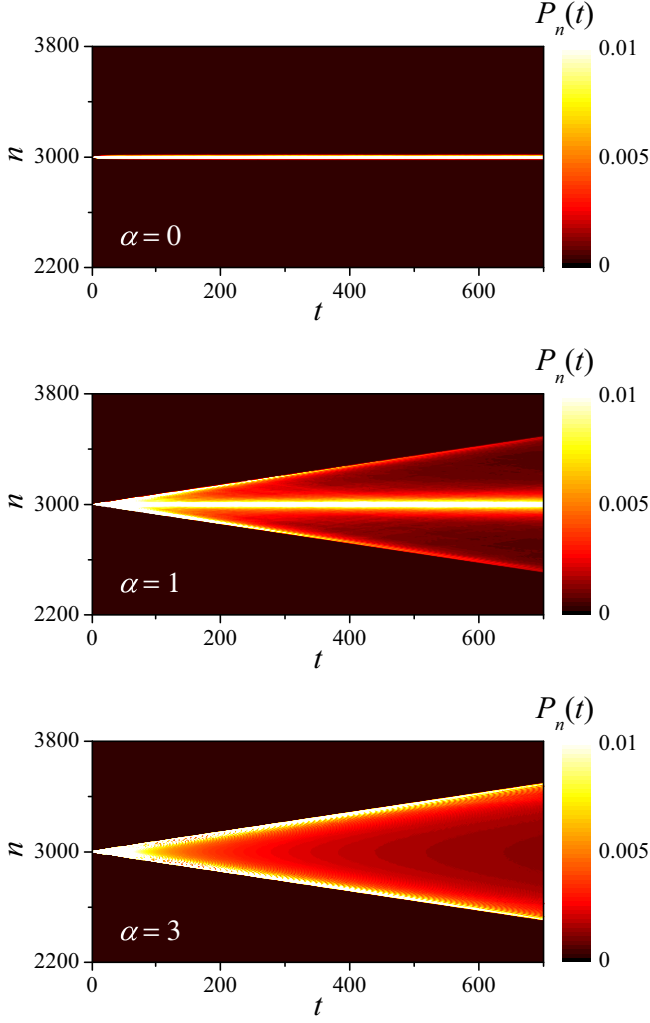


FIG. 2. Time evolution of the wave-packet probability distribution $P_n(t)$ versus n and t for $\alpha = 0, 1$, and 3 averaged over 10^3 realizations of disorder. For weak correlations ($\alpha = 0$ and 1) a finite fraction of the walker remains localized around the initial position $n_0 = N/2 = 3000$. For $\alpha = 3$ the state acquires a delocalized-like behavior.

detailed investigation into the dynamics of the disordered DTQW.

III. RESULTS AND DISCUSSION

In the following we discuss our results based on numerical simulations of the disordered quantum walk. In all figures displayed hereafter, the initial state is a symmetric one of the form $|\psi(t=0)\rangle = \frac{1}{\sqrt{2}}|\uparrow, n_0\rangle + \frac{i}{\sqrt{2}}|\downarrow, n_0\rangle$ with $n_0 = N/2$.

Let us first take a look over the dynamics profile of the walker upon varying α . In Fig. 2 we plot the time evolution of $P_n(t)$ versus n and t for $\alpha = 0, 1$, and 3 in an open chain. We observe that for $\alpha = 0$ the walker remains trapped around the initial position n_0 as expected since this case represents a quantum walk evolving in a chain with uncorrelated disorder. As widely known [28,31,35,37–41], disordered DTQWs share some similarities with the standard Anderson localization theory, meaning that the random scattering of the wave packet

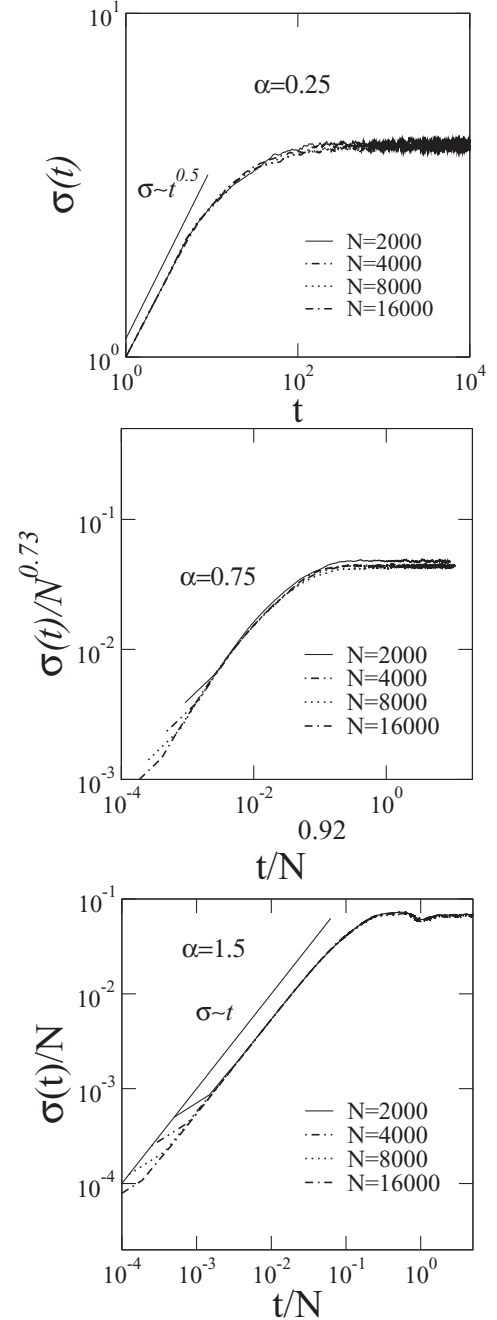


FIG. 3. $\sigma(t)$ versus t for $\alpha = 0.25, 0.75$, and 1.5 averaged over 10^3 distinct samples. For $\alpha = 1.5$ the walker wave-packet width exhibits ballistic dynamics with $\sigma \propto t$ before saturating due to finite-size effects. Data collapse is obtained by rescaling the width and time linearly by the chain size. Note that for $\alpha = 0.25$, σ is size independent. For $\alpha = 0.75$, data collapse is seen after properly rescaling the width and time by a sublinear power of the chain size.

leads to exponential localization of the quantum walker. This scenario changes when long-range correlations are added into disorder. For $\alpha = 1$ we already note that a fraction of the probability spreads within the chain while another finite fraction of the initial wave packet remains trapped around the initial site. For $\alpha = 3$ the wave-packet probability profile readily suggests delocalization of the quantum walker. We can see that the

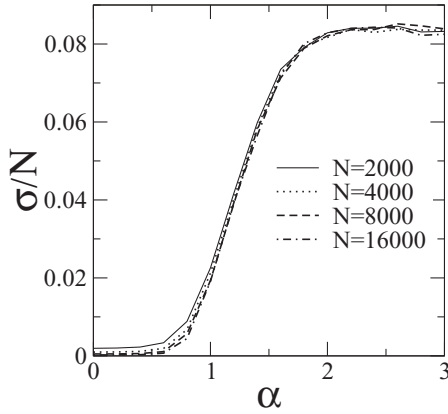


FIG. 4. Scaled long-time wave-function width $\sigma(t = 5N)/N$ versus α for $N = 2000$ to $16\,000$ averaged over 10^3 distinct disorder samples. Note that σ/N remains finite and size independent for large α .

wave front advances linearly in time, and the fraction of wave packet around the initial position (return probability) becomes vanishingly small. Those findings are preliminary indications that the walker wave function acquires an extended behavior.

A more precise description, though, can be obtained by analyzing the evolution of the wave-packet width in chains with distinct sizes. In Fig. 3 we plot $\sigma(t)$ versus t for three representative values of α and chain sizes $N = 2000$ to $16\,000$. In the small α regime ($\alpha = 0.25$), the width σ is size independent and saturates after an initial diffusive spreading. In the intermediate regime ($\alpha = 0.75$) the wave-packet width presents a sublinear size dependence. Data from distinct chain sizes are fairly collapsed by using proper width and time scales. The last panel accounts for the regime of large α , represented by $\alpha = 1.5$. In this case the wave-packet asymptotic width scales linearly with the system size after an initial ballistic spreading at which the wave packet displays a constant speed

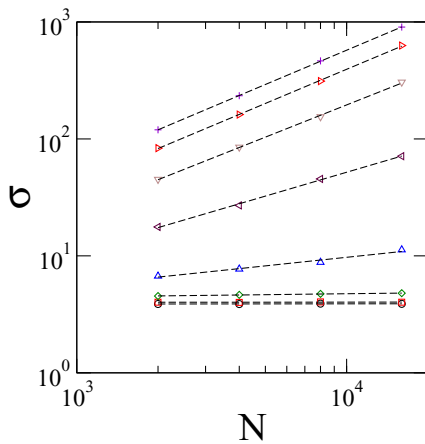


FIG. 5. Size dependence of the long-time wave-function width $\sigma(t = 5N)$ versus N for $\alpha = 0, 0.2, 0.4, 0.6, 0.8, 1.0, 1.2, 1.4$ (from bottom to top). The crossover from the size independent to the linear scaling regime can be effectively described by a sublinear power-law behavior of the form $\sigma \propto N^\Sigma$.

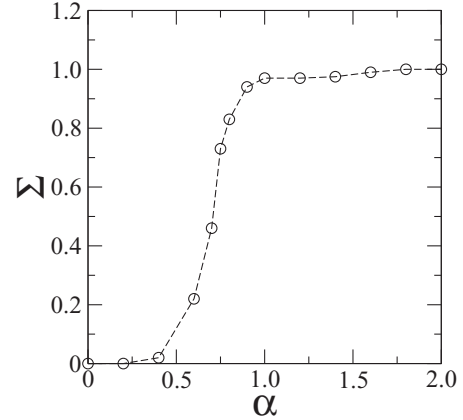


FIG. 6. Finite-size scaling exponent of the wave-packet width $\sigma \propto N^\Sigma$, with $\sigma = \sigma(t = 5N)$. The power-law exponents are estimated for sizes $N = 2000$ to $16\,000$. We note three distinct regimes: (1) full localization with $\Sigma = 0$; (2) sublinear scaling with $0 < \Sigma < 1$; and (3) full delocalization with $\Sigma = 1$.

$v(\alpha = 1.5) \simeq 0.54$. Data collapse is now achieved by scaling both width and time linearly with the system size.

In order to talk about the boundaries of each dynamical regime described above more precisely, we turn our attention to the long-time behavior of the wave-packet width. Considering that the statistically stationary state in the ballistic regime is reached for $t/N > 1$, we evaluate the wave-packet width around $t = 5N$ by averaging it over 100 time steps and 1000 distinct disorder configurations. Figure 4 shows the scaled long-time behavior of the walker’s wave-function width σ/N versus α . This gives further support to the above indication that the wave-packet width remains finite for small values of α while scaling linearly with the system size for large values of α . In Fig. 5 we show in a log-log scale the size dependence of the wave-packet width for values of α within interval $[0, 1.4]$ and chain sizes ranging from $N = 2000$ to $N = 16\,000$. There we clearly see that the crossover from the size-independent to the linear regime can be well

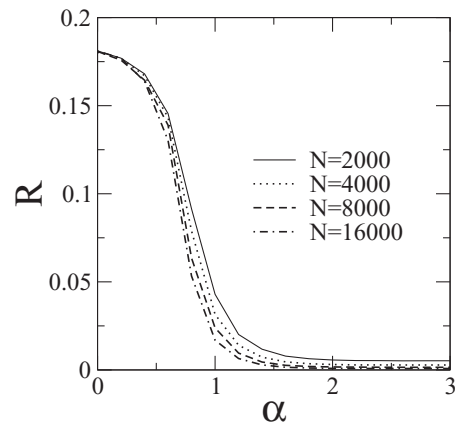


FIG. 7. Long-time behavior of the return probability $R = P_{n_0}(t = 5N)$ versus α for $N = 2000$ to $16\,000$ averaged over 10^3 distinct disorder samples. Note that the return probability remains finite and does not depend on the system size for $\alpha < 1/2$.

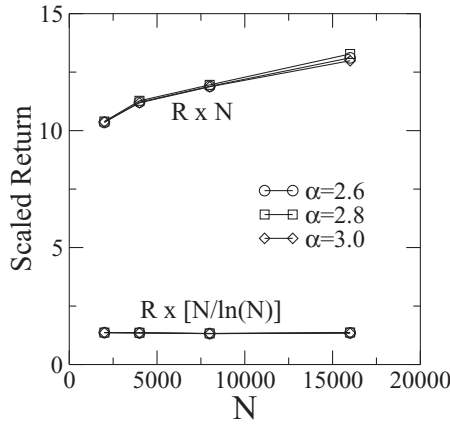


FIG. 8. Size dependence of RN and $RN/\ln N$ as a function of the chain size for representative values of α in the strongly correlated regime. The size independence of $RN/\ln N$ readily tells us how relevant this logarithmic correction is.

represented by an intermediate profile in which the wave-packet width depicts an effective sublinear finite-size scaling as $\sigma \propto N^\Sigma$, with $0 < \Sigma < 1$. The estimated values of the effective exponent Σ as a function of α are plotted in Fig. 6. It shows that the regime at which the wave packet remains fully localized, i.e., $\Sigma = 0$, persists up to $\alpha \simeq 0.5$. The fully extended state, corresponding to $\Sigma = 1$, emerges when $\alpha > 1$. In the range $0.5 < \alpha < 1$ the wave packet exhibits a sublinear finite-size scaling, signaling weak localization.

Further scaling analysis can also be performed for another very relevant property of the wave-packet dynamics, namely, its return probability $R(t) = P_{n_0}(t)$. In Fig. 7 we plot its statistically stationary value as a function of α obtained from distinct chain sizes. The return probability remains finite for small values of α and vanishes as it increases, in agreement with the localization-delocalization transition reported above. In order to unveil the finite-size scaling behavior of the return probability in the strongly correlated regime, we plot RN as well as $RN/\ln N$ as a function of the chain size in Fig. 8. There one observes that the proper scaling variable is the one that takes a logarithmic correction to the linear scaling into account, thus yielding a size-independent behavior. This very result indicates that in the strongly correlated regime the asymptotic return probability decays as $R \propto \ln(N)/N$.

Now taking $\tilde{N} = N/\ln N$ as the (more appropriate) scaling variable, we explore the size dependence of the return probability for a wide range of α . Our results are summarized in Fig. 9. Note that the crossover from the size independent to the linear scaling (with a logarithmic correction) regime can also be effectively described by an intermediate sublinear power-law scaling regime on which $R \propto \tilde{N}^\beta$, with $0 < \beta < 1$. The estimated values for the scaling exponent β are reported in Fig. 10. In the fully localized regime ($\alpha < 0.5$), the return scaling exponent $\beta = 0$, as expected. However, differently from the linear scaling behavior of the wave-packet width σ that develops at $\alpha = 1$, the linear scaling of the return probability is reached only for higher values of α .

Due to the *intrinsic* logarithmic correction to scaling of the return probability, numerical calculations carried out for

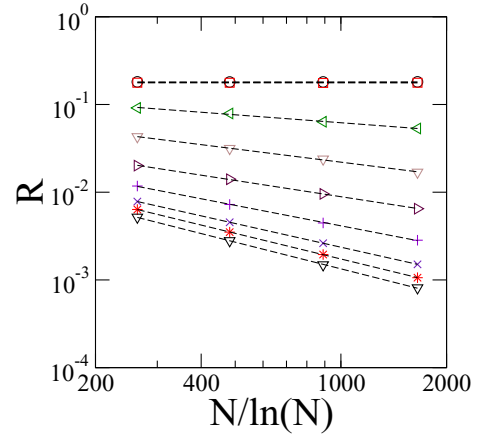


FIG. 9. Return probability R versus scaling variable $N/\ln N$ for $\alpha = 0, 0.2, 0.8, 1.0, 1.2, 1.4, 1.6, 1.8, 3.0$ (from top to bottom). The intermediate scaling regime can be effectively represented by a sublinear power law $R \propto \tilde{N}^{-\beta}$ with $0 < \beta < 1$.

larger chain sizes would be necessary to accurately determine the upper bound of the regime with sublinear, finite-size scaling of the return probability. However, we conjecture that the exact bounds for the regimes reported above are directly related to the distinct statistical regimes of the underlying random phase landscape. When $\alpha < 1/2$ the phase sequence is stationary, thus leading to full localization. For nonstationary phase sequences with antipersistent increments, $1/2 < \alpha < 1$, one gets weak localization of the quantum walk wave function with a sublinear finite-size scaling of the wave-packet width. Localization also develops for phase sequences with persistent increments, $\alpha > 1$, which leads to the linear scaling of $\sigma \propto N$. However, a roughly uniform, statistically stationary wave-packet profile is reached only when the fractal character of the underlying phase landscape is lost, which makes disorder

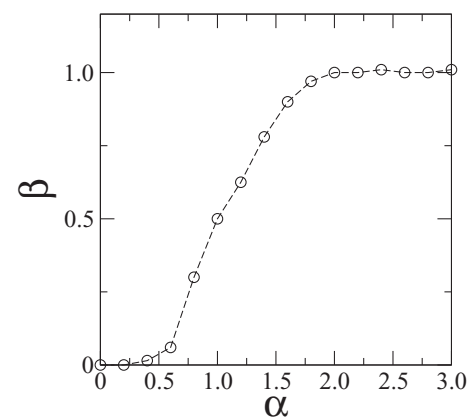


FIG. 10. Finite-size scaling exponent of the return probability $R \propto 1/\tilde{N}^\beta$, with $R = P_{n_0}(t = 5N)$, for $N = 2000, 4000, 8000$, and $16\,000$. Here $\tilde{N} = N/\ln N$. For each α and N we averaged $P_{n_0}(t)$ over 10^3 distinct realizations of disorder, picked out the last 100 steps before $t = 5N$, and then took another average to finally set R . We note three distinct regimes: (1) $\beta = 0$; (2) $0 < \beta < 1$; and (3) $\beta = 1$ (signaling a linear behavior with logarithmic correction). An intermediate, sublinear regime develops in the range $1/2 < \alpha < 3/2$.

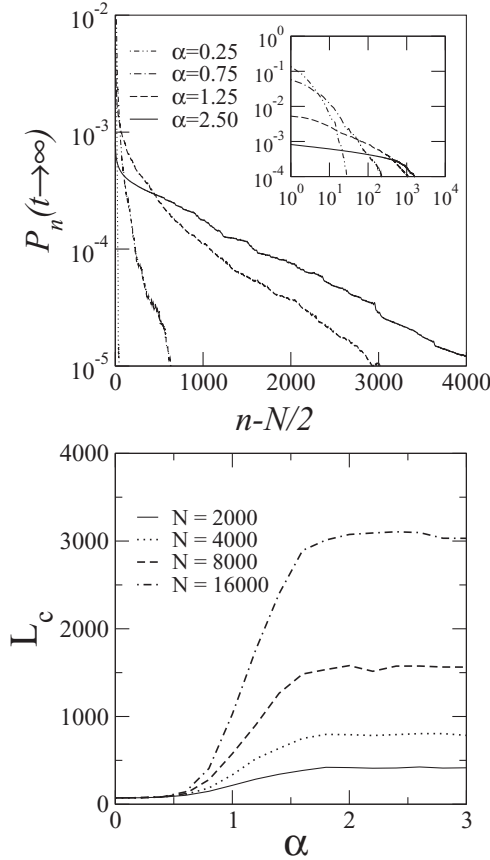


FIG. 11. Top: long-time wave-packet profile for some representative values of the correlation exponent α . The local occupation probability P_n was evaluated at $t = 5N$ with $N = 16000$. The main panel shows the development of an exponential tail while the inset emphasizes the power-law decay at intermediate values of α prior to the exponential cutoff. Bottom: cutoff length L_c versus α for various sizes N averaged over 10^3 distinct realizations of disorder. While the cutoff is size independent for $\alpha < 1/2$, it scales linearly with the system size for $\alpha > 3/2$.

irrelevant. This is the case for $\alpha > 3/2$ whereupon the return probability scales almost linearly with the chain size. The slight deviation from the linear scaling near $\alpha = 3/2$ suggests that much larger chain sizes would be required to accurately capture the asymptotic scaling in the vicinity of this point.

Last, in order to go deeper towards understanding the several scenarios unveiled by the finite-size scaling behavior, we plot the wave-packet profile after a large number of steps in the top panel of Fig. 11 for some representative values of α . For small degree of correlations ($\alpha < 1/2$), the wave packet remains strongly localized around the initial position. Above this value, the wave packet develops a slowly decaying power-law behavior interrupted by an exponential

cutoff. Then the wave packet gets about a flat profile for $\alpha > 3/2$ —presenting a very slow decay followed by the cutoff—thereby reaching the ultimate delocalized regime. In this case, $\sigma \propto N$ while $R \propto \ln N/N$. In the bottom panel of Fig. 11 we display the cutoff length L_c against α for various N . The cutoff is estimated as the distance to the initial position at which the statistically stationary wave function becomes smaller than 10^{-30} . For $\alpha < 1/2$ the cutoff is size independent while it reaches a plateau for $\alpha > 3/2$ on which $L_c \propto N$.

IV. CONCLUDING REMARKS

In this work we unveiled the dynamics of a disordered DTQW featuring long-range correlations controlled by a single parameter, α , displaying a power-law spectrum of the form $1/k^{2\alpha}$. Our results showed that ballistic dynamics is maintained in the presence of disorder provided the degree of correlations is high enough. Four distinct regimes were identified from the finite-size scaling analysis of the wave-packet width σ and the return probability. Strong localization persists for $\alpha < 1/2$, when the underlying random phase landscape is stationary. The usual regime of nearly uniform delocalization sets in for $\alpha > 3/2$ reflecting the nonfractal aspect of the phase distribution. We also identified the existence of two intermediate regimes on which the wave packet develops a slowly decaying power-law tail. Whenever the random phase landscape has antipersistent increments ($1/2 < \alpha < 1$) the quantum walker presents weak delocalization, with σ scaling sublinearly with the chain size. For nonstationary phase sequences with persistent increments ($1 < \alpha < 3/2$), σ spans over a finite fraction of the chain, although the return probability still scales sublinearly.

Our work builds upon the impact of Anderson localization-delocalization transitions in DTQWs. Quantum walks are convenient platforms for quantum simulation [26,35,40,41], and the role of different kinds of noise must be taken into account, such as those able to drive a Anderson localization breakdown [45]. The interplay between localized and delocalized dynamics can also be very useful in the realm of quantum communication protocols [54,55].

Further extensions of our work can be carried out by considering the effects of coin disorder [26] and the overall relationship between localization properties and the underlying topological phases [32]. Another direction can be taken towards studying the dynamics of many-particle quantum walk [13] against correlated disorder.

ACKNOWLEDGMENTS

This work was partially supported by CNPq, CAPES, FINEP, CNPq-Rede Nanobioestruturas, and FAPEAL (Alagoas State Agency).

[1] Y. Aharonov, L. Davidovich, and N. Zagury, *Phys. Rev. A* **48**, 1687 (1993).
 [2] J. Kempe, *Contemp. Phys.* **44**, 307 (2003).
 [3] S. E. Venegas-Andraca, *Quant. Info. Proc.* **11**, 1015 (2012).

[4] N. Shenvi, J. Kempe, and K. B. Whaley, *Phys. Rev. A* **67**, 052307 (2003).
 [5] A. M. Childs and J. Goldstone, *Phys. Rev. A* **70**, 022314 (2004).

- [6] T. G. Wong, K. Wünscher, J. Lockhart, and S. Severini, *Phys. Rev. A* **98**, 012338 (2018).
- [7] A. M. Childs, *Phys. Rev. Lett.* **102**, 180501 (2009).
- [8] N. B. Lovett, S. Cooper, M. Everitt, M. Trevers, and V. Kendon, *Phys. Rev. A* **81**, 042330 (2010).
- [9] E. Farhi and S. Gutmann, *Phys. Rev. A* **58**, 915 (1998).
- [10] C. A. Ryan, M. Laforest, J. C. Boileau, and R. Laflamme, *Phys. Rev. A* **72**, 062317 (2005).
- [11] H. Schmitz, R. Matjeschk, C. Schneider, J. Glueckert, M. Enderlein, T. Huber, and T. Schaetz, *Phys. Rev. Lett.* **103**, 090504 (2009).
- [12] H. B. Perets, Y. Lahini, F. Pozzi, M. Sorel, R. Morandotti, and Y. Silberberg, *Phys. Rev. Lett.* **100**, 170506 (2008).
- [13] L. Sansoni, F. Sciarrino, G. Vallone, P. Mataloni, A. Crespi, R. Ramponi, and R. Osellame, *Phys. Rev. Lett.* **108**, 010502 (2012).
- [14] E. Flurin, V. V. Ramasesh, S. Hacoheh-Gourgy, L. S. Martin, N. Y. Yao, and I. Siddiqi, *Phys. Rev. X* **7**, 031023 (2017).
- [15] A. Romanelli, *Phys. Rev. A* **80**, 042332 (2009).
- [16] D. Meyer, *J. Stat. Phys.* **85**, 551 (1996).
- [17] Y. Omar, N. Paunković, L. Sheridan, and S. Bose, *Phys. Rev. A* **74**, 042304 (2006).
- [18] P. K. Pathak and G. S. Agarwal, *Phys. Rev. A* **75**, 032351 (2007).
- [19] P. P. Rohde, A. Schreiber, M. Štefaňák, I. Jex, and C. Silberhorn, *New J. Phys.* **13**, 013001 (2011).
- [20] P. Xue and B. C. Sanders, *Phys. Rev. A* **85**, 022307 (2012).
- [21] L. Rigovacca and C. Di Franco, *Sci. Rep.* **6**, 22052 (2016).
- [22] A. Schreiber, A. Gábris, P. P. Rohde, K. Laiho, M. Štefaňák, V. Potoček, C. Hamilton, I. Jex, and C. Silberhorn, *Science* **336**, 55 (2012).
- [23] J. K. Gamble, M. Friesen, D. Zhou, R. Joynt, and S. N. Coppersmith, *Phys. Rev. A* **81**, 052313 (2010).
- [24] S. D. Berry and J. B. Wang, *Phys. Rev. A* **83**, 042317 (2011).
- [25] V. Kendon, *Math. Struct. Comp. Sci.* **17**, 1169 (2007).
- [26] C. M. Chandrashekar, *Phys. Rev. A* **74**, 032307 (2006).
- [27] P. M. Preiss, R. Ma, M. E. Tai, A. Lukin, M. Rispoli, P. Zupancic, Y. Lahini, R. Islam, and M. Greiner, *Science* **347**, 1229 (2015).
- [28] H. Obuse and N. Kawakami, *Phys. Rev. B* **84**, 195139 (2011).
- [29] T. Kitagawa, M. A. Broome, A. Fedrizzi, M. S. Rudner, E. Berg, I. Kassal, A. Aspuru-Guzik, E. Demler, and A. G. White, *Nat. Commun.* **3**, 882 (2012).
- [30] T. Kitagawa, *Quant. Info. Proc.* **11**, 1107 (2012).
- [31] T. Rakovszky and J. K. Asboth, *Phys. Rev. A* **92**, 052311 (2015).
- [32] J. M. Edge and J. K. Asboth, *Phys. Rev. B* **91**, 104202 (2015).
- [33] A. Wójcik, T. Łuczak, P. Kurzyński, A. Grudka, T. Gdala, and M. Bednarska-Bzdęga, *Phys. Rev. A* **85**, 012329, (2012).
- [34] R. Zhang, P. Xue, and J. Twamley, *Phys. Rev. A* **89**, 042317 (2014).
- [35] F. De Nicola, L. Sansoni, A. Crespi, R. Ramponi, R. Osellame, V. Giovannetti, R. Fazio, P. Mataloni, and F. Sciarrino, *Phys. Rev. A* **89**, 032322 (2014).
- [36] J. Ghosh, *Phys. Rev. A* **89**, 022309 (2014).
- [37] Q. Zhao and J. Gong, *Phys. Rev. B* **92**, 214205 (2015).
- [38] I. Vakulchyk, M. V. Fistul, P. Qin, and S. Flach, *Phys. Rev. B* **96**, 144204 (2017).
- [39] M. Zeng and E. H. Yong, *Sci. Rep.* **7**, 12024 (2017).
- [40] A. Schreiber, K. N. Cassemiro, V. Potoček, A. Gábris, I. Jex, and C. Silberhorn, *Phys. Rev. Lett.* **106**, 180403 (2011).
- [41] A. Crespi, R. Osellame, R. Ramponi, V. Giovannetti, R. Fazio, L. Sansoni, F. De Nicola, F. Sciarrino, and P. Mataloni, *Nat. Photon.* **7**, 322 (2013).
- [42] R. Vieira, E. P. M. Amorim, and G. Rigolin, *Phys. Rev. Lett.* **111**, 180503 (2013).
- [43] R. Vieira, E. P. M. Amorim, and G. Rigolin, *Phys. Rev. A* **89**, 042307 (2014).
- [44] Q.-Q. Wang, X.-Y. Xu, W.-W. Pan, K. Sun, J.-S. Xu, G. Chen, Y.-J. Han, C.-F. Li, and G.-C. Guo, *Optica* **5**, 1136 (2018).
- [45] F. A. B. F. de Moura and M. L. Lyra, *Phys. Rev. Lett.* **81**, 3735 (1998).
- [46] D. H. Dunlap, H.-L. Wu, and P. W. Phillips, *Phys. Rev. Lett.* **65**, 88 (1990).
- [47] P. Phillips and H.-L. Wu, *Science* **252**, 1805 (1991).
- [48] F. M. Izrailev and A. A. Krokhin, *Phys. Rev. Lett.* **82**, 4062 (1999).
- [49] R. P. A. Lima, M. L. Lyra, E. M. Nascimento, and A. D. de Jesus, *Phys. Rev. B* **65**, 104416 (2002).
- [50] F. A. B. F. de Moura, M. D. Coutinho-Filho, E. P. Raposo, and M. L. Lyra, *Phys. Rev. B* **66**, 014418 (2002).
- [51] F. A. B. F. de Moura, M. D. Coutinho-Filho, E. P. Raposo, and M. L. Lyra, *Phys. Rev. B* **68**, 012202 (2003).
- [52] F. Domínguez-Adame, V. A. Malyshev, F. A. B. F. de Moura, and M. L. Lyra, *Phys. Rev. Lett.* **91**, 197402 (2003).
- [53] J. Rodríguez-Laguna, S. N. Santalla, G. Ramirez, and G. Sierra, *New J. Phys.* **18**, 073025 (2016).
- [54] G. M. A. Almeida, F. A. B. F. de Moura, T. J. G. Apollaro, and M. L. Lyra, *Phys. Rev. A* **96**, 032315 (2017).
- [55] G. M. A. Almeida, F. A. B. F. de Moura, and M. L. Lyra, *Phys. Lett. A* **382**, 1335 (2018).
- [56] U. Kuhl, F. M. Izrailev, A. A. Krokhin, and H.-J. Stockmann, *Appl. Phys. Lett.* **77**, 633 (2000).
- [57] U. Kuhl, F. M. Izrailev, and A. A. Krokhin, *Phys. Rev. Lett.* **100**, 126402 (2008).
- [58] L. D. da Silva, A. Ranciaro Neto, M. O. Sales, M. L. Lyra, and F. A. B. F. de Moura, *Physica A* **486**, 895 (2017).
- [59] B. B. Mandelbrot and J. R. Wallis, *Water Resour. Res.* **5**, 228 (1969).